

Determination of Material Parameters for Discrete Damage Mechanics Analysis of Carbon-Epoxy Laminates

E. J. Barbero¹

Cátedra de Excelencia, Universidad Carlos III de Madrid, Spain.

and

F. A. Cossio²

Mechanical and Aerospace Engineering, West Virginia University,
Morgantown, WV 26506-6106, USA

Abstract

Discrete damage mechanics (DDM) refers to micromechanics of damage constitutive models that, when incorporated into commercial finite element software via user material subroutines, are able to predict intralaminar transverse and shear damage initiation and evolution in terms of the fracture toughness of the composite. A methodology for determination of the fracture toughness is presented, based on fitting DDM model results to available experimental data. The applicability of the DDM model is studied by comparison to available experimental data for Carbon Epoxy laminates. Sensitivity of the DDM model to h- and p-refinement is studied. Also, prediction of modulus vs. applied strain is contrasted with ply discount results and the effect of in situ correction of strength is highlighted.

keyword

A. Polymer-matrix composites (PMCs); B. Transverse cracking; C. Damage mechanics; C. Finite element analysis (FEA); Parameter Identification.

1 Introduction

Prediction of damage initiation and accumulation in polymer matrix, laminated composites is of great interest for the design, production, certification, and monitoring of an increasingly large variety of structures. Matrix cracking due to transverse tensile and shear deformations is considered in this manuscript. Matrix cracking is normally the first mode of damage and, if left unmitigated often leads to other modes such as delamination, and even fiber failure of adjacent laminas due to

¹Corresponding author. The final publication is available at <http://dx.doi.org/10.1016/j.compositesb.2013.08.084>

²Graduate Research Assistant.

load redistribution. Furthermore, extensive cracking leads to increased permeability and exposes the fibers to deleterious environmental attack.

The earliest, simplest and least accurate modeling technique to address matrix damage is perhaps the ply discount method [1, Section 7.3.1]. Ply discount is used in this work as a baseline for contrasting predictions obtained with the Discrete Damage Mechanics (DDM) method. Although many other models exist, such as [2, 3, 4, 5, 6, 7, 8, 9, 10, 11, 12], Abaqus PDA [13, 14, 15], and several plugins [16, 17], this manuscript focuses on DDM because its inherent features make it attractive.

Briefly, DDM [18] is a constitutive modeler that is inherently mesh independent, thus not requiring the user to choose a *characteristic length*. Furthermore, only two material parameters, the fracture toughness in modes I and II, are required to predict both initiation and evolution of transverse and shear damage. Since transverse and shear strengths are not used to predict damage initiation, but rather fracture toughness is used, DDM automatically accounts for in situ effects. No additional parameters are required to predict damage evolution. Also, as it is shown in this work, DDM parameters can be identified for Carbon fiber composites. This is not easily done for continuum damage mechanics (CDM) models because their state variables, namely the damage variables, are not measurable [19]. As a result, one is faced with identifying the model parameters using a macroscopic effect, such as the experimentally measured loss of stiffness, which for Carbon fiber composites is small [20]. Finally, DDM is available to be used in conjunction with commercial FEA environments such as Abaqus³ [15] and ANSYS/Mechanical⁴ [21], in the form of UMAT, UGENS [22], and USERMAT [23].

Therefore, the objective of this manuscript is to propose a methodology to determine values for the material properties required by the DDM model. In this work, the values for the parameters are found using available experimental data and a rational procedure. Once values are found, the DDM model is applied for predicting other, independent results, and conclusions are drawn about the applicability of the model.

No standard test method exist to measure the intralaminar fracture toughness. Although standards exist for measuring interlaminar fracture toughness in mode I (ASTM D5528) and proposed methods exist for mode II [24, 25], intralaminar properties are not the same as interlaminar ones. Thus the need for a method to find the intralaminar fracture toughness using available data for a broad set of material systems.

2 Discrete Damage Mechanics

Given the crack density and the shell strain, DDM [18] updates the state variable, i.e., the crack density, and calculates the shell stress resultant and secant stiffness matrix A, B, D , and/or the tangent stiffness matrix, all of them functions of crack density. The crack density λ is an array containing the crack density for all the laminas at an integration point of the shell element. The strain refers to the shell strain array ϵ, κ , conjugate to the shell stress resultant array N, M . In this way, DDM is a constitutive model that can be implemented as a user material subroutine (UMAT, VUMAT, USERMAT) [23, usermatps-901] for flat plane stress elements and as a user general section (UGENS) for curved shell elements [22, ugens-std].

³Abaqus and Simulia are trademarks or registered trademarks of Dassault Systèmes or its subsidiaries in the United States and/or other countries.

⁴Ansys® is a registered trademark of ANSYS Inc.

2.1 Damage Initiation and Evolution

Damage initiation and evolution are controlled by a single equation representing the Griffith's criterion for an intralaminar crack, i.e., the undamaging domain is defined by

$$g(\epsilon, \lambda) = \max \left[\frac{G_I(\epsilon, \lambda)}{G_{IC}}, \frac{G_{II}(\epsilon, \lambda)}{G_{IIC}} \right] - 1 \leq 0 \quad (1)$$

where G_I, G_{II} are the strain energy release rates (ERR) in modes I and II, calculated with (15)-(16), and G_{IC}, G_{IIC} are the invariant material properties representing the energy necessary to create a new crack. We shall see that for fixed strain, both G_I, G_{II} are decreasing functions of λ . Therefore, (1) exhibits strain-hardening as a function of crack density λ , and thus stress-softening as a function of strain ϵ .

DDM calculates G_I, G_{II} using a micromechanics of damage model that reduces the 3D equilibrium equations

$$\frac{\partial \sigma_i}{\partial x_j} + f_i = \rho \frac{\partial^2 u_i}{\partial t^2} \quad ; \quad i, j = 1 \dots 3 \quad (2)$$

to 2D using the following approximations. First, a state of plane stress for symmetric laminates under membrane loads allows us to eliminate the u_3 component of the displacement, by using the following

$$\sigma_3 = 0 \quad (3)$$

$$\frac{\partial u_3}{\partial x_i} = 0 \quad ; \quad i = 1, 2 \quad (4)$$

Then, (2) are recast in terms of the thickness average of the displacements in each lamina defined as follows

$$\hat{u}_i^{(k)} = \int_{-h_k/2}^{h_k/2} u_i(z) dz \quad ; \quad i = 1, 2 \quad (5)$$

where h_k is the thickness of lamina k . Next, the intralaminar shear stress components τ_{j3} , with $j = 1, 2$, are assumed to vary linearly in each lamina

$$\tau_{j3}^{(k)}(x_3) = \tau_{j3}^{k-1,k} + \left(\tau_{j3}^{k,k+1} - \tau_{j3}^{k-1,k} \right) \frac{x_3 - x_3^{k-1,k}}{h_k} \quad ; \quad j = 1, 2 \quad (6)$$

With these assumptions, the 3D equilibrium equations (2) reduce to a system of $2n$ partial differential equations in 2D, with 2 equations per lamina, in terms of displacements, where n is the number of laminas in the laminate.

Experimental [26] and theoretical considerations [1, § 7.2.1] support the assumption of periodically spaced cracks that propagate suddenly, in an unstable fashion, through the thickness of the lamina and along the fiber direction. Therefore, the domain is that of a representative volume element (RVE) spanning the laminate thickness, between two adjacent cracks, as shown in Fig. 1. The length $2l$ of the RVE is inversely proportional to the crack density, i.e.,

$$\lambda = 1/2l \quad (7)$$

where $2l$ is the distance between two cracks.

In this way, the crack density enters the model through the length of the RVE. Since the ERR is computed in this RVE, which is independent of the finite element discretization, coupled to the fact that the constitutive model is formulated in terms of displacements rather than strains, the constitutive model is inherently mesh independent, without the need for choosing a characteristic length. Such mesh independence is corroborated by numerical results by plotting the reaction force vs. applied displacement on the boundary.

The PDE system is then solved with the following boundary conditions:

- Free stress boundary at the cracked surfaces. The surface of the cracks in lamina c , located at $x = \pm l$, are free boundaries, and thus subject to zero stress, with zero resultant force, as follows

$$h_c \int_{-1/2}^{1/2} \hat{\sigma}_j^{(c)}(x_1, l) dx_1 = 0 \quad ; \quad j = 2, 6 \quad (8)$$

where h_c is the thickness of the cracked lamina.

- Displacement compatibility. All laminas $m = 1..n$ with n being the number of laminas, and $m \neq c$, that is, excluding the cracking lamina c , undergo the same displacement at the boundaries $(-l, l)$ when subjected to a membrane state of strain. Taking an arbitrary lamina $r \neq c$ as a reference, the remainder displacements are constrained as follows:

$$\hat{u}_j^{(m)}(x_1, \pm l) = \hat{u}_j^{(r)}(x_1, \pm l) \quad ; \quad \forall m \neq c \quad ; \quad j = 1, 2 \quad (9)$$

- Equilibrium. The stress resultant from the internal stress equilibrates the applied load.

In the direction parallel to the surface of the cracks (fiber direction x_1) the load N_1 is supported by all the laminas

$$\frac{1}{2l} \sum_{k=1}^N h_k \int_{-l}^l \hat{\sigma}_1^{(k)}(1/2, x_2) dx_2 = N_1 \quad (10)$$

In the direction normal to the crack surface (x_2 direction) only the uncracked laminas $m \neq c$ carry normal and shear loads

$$\sum_{m \neq k} h_m \int_{1/2}^{1/2} \hat{\sigma}_j^{(m)}(x_1, l) dx_1 = N_j \quad ; \quad j = 2, 6 \quad (11)$$

The solution of the PDE system yields the displacements in all laminas $\hat{u}_i^{(k)}$, and by differentiation, the strains in all laminas. Next, the compliance S of the laminate is calculated by solving three canonical load cases

$${}^a N/t = \begin{Bmatrix} 1 \\ 0 \\ 0 \end{Bmatrix}; \quad {}^b N/t = \begin{Bmatrix} 0 \\ 1 \\ 0 \end{Bmatrix}; \quad {}^c N/t = \begin{Bmatrix} 0 \\ 0 \\ 1 \end{Bmatrix} \quad (12)$$

where t is the thickness of the laminate. Since the three applied stress states are unit values, for each case, a , b , c , the volume average of the strain represents one column in the laminate compliance matrix

$$S = \begin{bmatrix} a\epsilon_x & b\epsilon_x & c\epsilon_x \\ a\epsilon_y & b\epsilon_y & c\epsilon_y \\ a\gamma_{xy} & b\gamma_{xy} & c\gamma_{xy} \end{bmatrix} \quad (13)$$

Next, the laminate in-plane stiffness $Q = A/t$ in the coordinate system of lamina k is

$$Q = S^{-1} \quad (14)$$

A fourth load case, namely $N = \{0, 0, 0\}^T$ and $\Delta T = 1$, allows us to get the degraded coefficient of thermal expansion (CTE) of the laminate. The resulting strain is equal to the CTE of the laminate, i.e., in this case, $\{\alpha_x, \alpha_y, \alpha_{xy}\}^T = \{\epsilon_x, \epsilon_y, \gamma_{xy}\}^T$.

Then, the ERR in fracture modes I and II are calculated as follows

$$G_I = -\frac{V_{RVE}}{2\Delta A} (\epsilon_2 - \alpha_2\Delta T) \Delta Q_{2j} (\epsilon_j - \alpha_j\Delta T) \quad ; \quad \text{opening mode} \quad (15)$$

$$G_{II} = -\frac{V_{RVE}}{2\Delta A} (\epsilon_6 - \alpha_6\Delta T) \Delta Q_{6j} (\epsilon_j - \alpha_j\Delta T) \quad ; \quad \text{shear mode} \quad (16)$$

where V_{RVE} , ΔA , are the volume of the RVE and the area of the new discrete crack, respectively.

Tearing mode III does not participate because out of plane displacements of the lips of the crack are constrained by the adjacent laminas in the laminate.

Once (1) can be calculated, the crack density is found using a return mapping algorithm (RMA) to satisfy $g = 0$, as follows

$$\Delta\lambda_k = -g_k / \frac{\partial g_k}{\partial \lambda} \quad (17)$$

The RMA (17) attempts to find the value of crack density λ that takes the damage activation function to $g = 0$ as per (1). The search is done at constant strain, inside the constitutive modeler for a given iteration of the structural analysis program. When the RMA reaches $g = 0$, the new crack density is now fixed to a value that is larger than before.

An increase of crack density produces a drop of stiffness Q , and stiffness rate ΔQ as well; thus, a drop of ERR as per (15)-(16). With the new crack density, the ERR is less than before. So, the value of g immediately drops below zero. This means that once the crack density found by the RMA is accepted, the system stops damaging unless the strain grows, but an increase of strain can be imposed by the structural analysis program in a subsequent iteration.

In other words, (15)-(16) displays strain hardening. To illustrate this, consider (15) for mode I. With reference to the dimensions of the RVE in Fig. 1, we have that $V_{RVE} = 2l \times 1 \times t$, where t is the thickness of the laminate. For each new crack, the crack area grows by $\Delta A = h_k \times 1$ and the crack density doubles, so that $\Delta\lambda = \lambda$. Finally, considering (7), and for a case of uniaxial state of stress in a tensile test, we have

$$G_I = \left(-\frac{t}{h_k} \frac{\Delta E}{2\Delta\lambda} \right) \epsilon^2 \quad (18)$$

where $E(\lambda)$ is the laminate modulus in the direction of the applied strain ϵ . At constant strain, a decreasing parenthesis in (18) assures that once the RMA has converged to a value of λ , no more damage can occur without an increase of strain. Variation of G_I/ϵ^2 vs. crack density is shown in Fig. 2 for laminates 2, 9, and 10 (Table 1).

Next, considering increasing strain, as soon as cracks appear, dissipation takes place, and its value is shown in Fig. 3 for the three materials considered. Note however that values in these charts are not normalized by the thickness of the laminate.

Once the degraded stiffness of the laminate (14) is known, the degraded stiffness of the cracked lamina, i.e., lamina c , can be computed as

$$Q^{(c)} = \frac{t}{h_c} \left[Q - \sum_{m=1}^n (1 - \delta_{mc}) Q^{(m)} \frac{h_m}{t} \right] \quad (19)$$

where t, h_i , are the thickness of the laminate and the thicknesses of the laminas, respectively.

Modulus degradation of the cracking lamina is shown in Fig. 4 and the stress carried by the cracking lamina is shown in Fig. 5. Assuming there is no elastic recovery, the area under each curve represents dissipation and it can be seen how the three materials compare in this regard. Furthermore, stress *softening* is clearly shown in Fig. 5. Note that, in contrast to Abaqus PDA [15, § 24.3], the remaining stress in the cracking lamina does not vanishes.

Since DDM is insensitive to characteristic length (see Section 6.3), Fig. 5 could be plotted in terms of a displacement δ obtained for example by multiplying the strain by the length of the specimen. Then, one would note the striking difference with the $\sigma - \delta$ plot assumed in Abaqus PDA [15, § 24.3], which assumes a linear decrease of σ after crack initiation (point A in Fig. 5 and [20, Fig. 1]), eventually dropping to zero stress. This means that in Abaqus PDA, the stress is controlled by an assumed (linear) softening equation. On the contrary, DDM makes no assumption about the shape of the of the softening curve. Instead, the softening curve is predicted by DDM (Fig. 5) in terms of the fracture toughness G_{Ic}, G_{IIc} , of the material.

One can confidently assume that the modulus of the cracking lamina decreases but it does not drop to zero. Once the residual modulus is multiplied by an increasing strain, it can be seen in Fig. 5 that the cracking lamina carries significant stress.

In Abaqus PDA, $\delta = l_c \epsilon$, where l_c is the characteristic length used to mitigate mesh dependency [15]. In Abaqus, such characteristic length is chosen as the square root of the area of the each element in the mesh. No characteristic length is necessary in DDM.

3 Ply Discount

The ply discount method was used to compare to the DDM prediction of loss of stiffness. The Hashin damage initiation criteria was implemented in a user subroutine based on (20), using nominal stress

$$F_m^t = \left(\frac{\sigma_{22}}{F_{2t}} \right)^2 + \left(\frac{\sigma_{12}}{F_6} \right)^2 \quad (20)$$

where F_{2t} is the tensile strength in the matrix direction and F_6 is the longitudinal shear strength [27]. Furthermore, $F_{mt} > 1$ indicates that the damage initiation criterion has been satisfied.

For damage evolution, the ply discount method simply reduces to zero the stiffness of the lamina that reaches the damage onset, except in the fiber direction which is left unchanged. In order to prevent convergence problems, the secant stiffness (22) is reduced using $d_f = 0, d_m = d_s = 0.999$, abruptly as soon as the Hashin damage initiation criteria (20) has been met. That is, the secant constitutive equation is

$$\sigma = C : \varepsilon \quad (21)$$

where σ is the apparent stress, ε is the strain, and the secant stiffness is given by

$$C = \begin{bmatrix} E_1/\Delta & (1-d_m)\nu_{21}E_1/\Delta & 0 \\ (1-d_m)\nu_{12}E_2/\Delta & (1-d_m)E_2/\Delta & 0 \\ 0 & 0 & (1-d_s)G_{12} \end{bmatrix} \quad (22)$$

$$\Delta = 1 - (1-d_f)(1-d_m)\nu_{12}\nu_{21} \quad (23)$$

where E_1, E_2 are the moduli in the fiber direction and perpendicular to the fibers, respectively, G_{12} is the inplane shear modulus, ν_{12}, ν_{21} , are the inplane and out of plane Poisson's ratios, and d_m, d_s are damage variables for transverse and shear damage modes, respectively. In absence of fiber damage, $d_s = d_m$ [20].

For ply discount, the values of strength, F_{2t}, F_6 are material properties that must be provided by the user. Due to differences between testing and application conditions, as well as in situ effects [1, Section 7.2.1], the strength values measured by standard methods may not predict damage initiation accurately. Therefore, in this work, the values of strength are found by calibrating model results to *laminated* experimental data.

Then, the stress is calculated with (21), where ε is total strain. In a nonlinear incremental analysis, $\varepsilon_i = \varepsilon_{i-1} + \Delta\varepsilon_i$, where i is the current step. If damage has not initiated, the damage initiation criteria is evaluated for the recently calculated values of stress to decide whether or not the damage initiation criteria has been met. In ply discount, damage evolution is sudden and abrupt, occurring simultaneously with damage initiation.

4 Available Experimental Data

Crack density λ vs. applied strain ε_x or applied stress $\sigma_x = N_x/t$, measured experimentally and reported in the literature, were used to compare with DDM and Ply Discount predictions. The laminate stacking sequences shown in Table 1 were considered [28]. The dimensions of the specimens are 12 mm wide with a free length of 110 mm. The material properties for the laminates are listed in Table 2.

All laminates were subjected to axial deformation ε_x , which coincides with ε_{11} in the 0° laminas. None of the laminas in these laminates is subjected to fiber modes or matrix compression. The 90° laminas are subjected to pure traction and no shear, so damage initiation is controlled by the parameter F_{2t} when a strength criterion is used and by G_{IC} when a fracture criterion is used.

5 Methodology

5.1 Strength Criterion

First ply failure (FPF) indicates the occurrence of the first transverse crack in the 90° lamina and it is controlled by the value of transverse tensile strength F_{2t} of a unidirectional lamina. This value is difficult to measure experimentally because of large scatter in the data. Literature values are given in Table 2 but they are assumed to be unreliable. Therefore, F_{2t} is *identified* in such a way that, for each laminate in Table 1, the calculated FPF load N_x equals the experimentally observed load $N_x = t\sigma_x$, where t is the thickness of the laminate and σ_x is the laminate stress reported from experiments. FPF is calculated with CLT [29] correcting the transverse tensile strength F_{2t} for in situ effect [1, (7.42)], as follows

$$F_{2t}^{insitu} = 1.12 \sqrt{\frac{2t_t}{t_e}} F_{2t} \quad (24)$$

where $t_e = \min(t_t, h_c)$; then, h_c is the thickness of the cracking lamina, and the transition thickness is taken as $t_t = 0.8$ mm, as it was found experimentally in [30], and fully explained in [1, (7.37)].

Values of transverse tensile strength F_{2t} identified in this way are reported in Table 2. For two of the materials reported, the values obtained are very close to the literature values, provided that in situ effect is taken into account in the prediction of FPF. Note the in situ values cannot be reported in tabular form because they are a function of ply thickness. Instead, one has to report the transverse tensile strength F_{2t} of the unidirectional (UD) lamina, as in Table 2, and rely on the software to adjust F_{2t}^{insitu} for each ply. This is not necessary with a fracture mechanics criterion, which uses the critical ERR as an invariant material property, and automatically accounts for in situ effect.

5.2 Fracture Mechanics Criterion

The value of critical energy release rate G_{IC} was obtained to provide a best fit with the DDM model to the experimental crack density λ vs. stress σ_x for laminates 2, 9, and 10 in Table 1. The experimental data and the fitted DDM model results are shown in Figs. 6, 8, and 10.

The error was calculated using the usual formula

$$Error = \frac{1}{n_e} \sqrt{\sum_{i=1}^{n_e} [\lambda^{model}(x_i) - \lambda^{experim}(x_i)]^2} \quad (25)$$

where $\lambda^{model}(x_i)$, $\lambda^{experim}$ are the predicted and experimental crack densities, respectively, x_i is the test progress indicator, be it stress or strain depending on how the experimental data is reported in the literature, and n_e is the number of experimental data points available.

By adjusting the parameter G_{IC} , the minimization algorithm converges to a global minimum. A MATLAB script was executed to look for the minimum error (25), by repeatedly executing Abaqus with parameters varying as per the Simplex method [31]. The converged values of G_{IC} are reported in Table 2.

All the laminates considered for the study are symmetric and balanced. Therefore a quarter of the specimen was used for the analysis using symmetry b.c. and applying a uniform strain via imposed displacements on one end of the specimen. A longitudinal displacement of 1.1 mm was applied to reach a strain of 2%. Abaqus S4R elements were used for most of the study but the convergence study also considered quadratic S8R elements, as well as ANSYS linear PLANE 182 and quadratic PLANE 183.

6 Model Assessment

6.1 Comparison with Experimental Data

In this section we compare crack density predicted with DDM vs. experimental data (Table 1). Figures 6, 8, and 11 merely state the fact that the values of G_{IC} are adjusted using the data for these laminates. Figures 7, 9, and 11 are new results, as the experimental data presented in them was not used to fit any parameters. It shows that the crack density is predicted well by the model.

Since the prediction of crack density (17) relies on accurate prediction of laminate stiffness (14), it can be inferred that the later is predicted with similar accuracy as the predicted crack density. Further, since the prediction of lamina stiffness (19) is directly related to the laminate stiffness, it has similar accuracy as the predicted crack density.

Experimental data reporting loss of laminate stiffness is scarce because the variation of stiffness is small, thus difficult to measure. For this reason, the critical ERR is identified with crack density data. However, stiffness loss is important because it determines the stress redistribution from the cracked lamina to the rest of the laminate, which as a result may reach a fiber dominated failure mode. To highlight the behavior of the DDM model, stiffness loss are compared to results obtained with the ply discount method.

6.1.1 Avimid® K Polymer/IM6

Laminate 2 was used to adjust G_{IC} because it shows the strongest mode I fracture behavior of the group. The result for the final iteration of the minimization algorithm is shown in Figure 6. Keeping the value of G_{IC} unchanged, laminates 1, 3, and 4 were simulated. The least favorable comparison of the group is for laminate 3, which has double amount of unidirectional and 50% less of transverse laminas, but still the comparison is acceptable as it can be seen in Figure 7.

A gradual loss of stiffness is observed in Figures 12-13. On the other hand, ply discount forces a sudden loss of stiffness, and thus underestimates the dissipated energy. Furthermore, according to the DDM predictions, and unlike ply discount, the cracking laminas have not lost entirely their stiffness for values of laminate stress that are likely to trigger fiber modes. Furthermore, the predictions are insensitive to the type of element used, namely linear S4R or quadratic S8R.

6.1.2 Fiberite 934/T300

Laminate 9 was used to adjust G_{IC} . The result for the final iteration of the minimization algorithm is shown in Figure 8. Keeping the value of G_{IC} unchanged, laminates 5, 6, 7, and 8 were simulated. Comparison with experimental data is shown in Figure 9.

A gradual loss of stiffness is observed in Figures 14-15, encompassing more dissipated energy than ply discount. Furthermore, the cracking laminas do not loose their stiffness entirely for values of laminate stress that are likely to trigger fiber modes. The predictions remain insensitive to the type of element used, namely linear S4R or quadratic S8R.

6.1.3 Hercules 3501-6/AS4

Laminate 10, which is the most susceptible to matrix cracking, was used to adjust G_{IC} . The result for the final iteration of the minimization algorithm is shown in Figure 10. Keeping the value of G_{IC} unchanged, laminate 11 was simulated. Comparison with experimental data are shown in Figure 11.

A gradual loss of stiffness is observed in Figures 16-17. Asymptotic behavior at large strains would be reached when the damage in the 90° lamina is fully developed and at such stage the laminate modulus with full discount of the cracking lamina would coincide with the ply discount prediction, but often this does not take place until large laminate stress/strain values that would have triggered fiber modes. Therefore, the ply discount model is unrealistic.

6.2 In situ Strength

Since the *identified* values of F_{2t} and F_6 , reported in Table 2, were calculated to match *laminate* data, the values obtained take into account in situ effects. To highlight the error incurred when using unidirectional (UD) lamina strength values rather than in situ values, a comparison is presented on Table 3 between the First Ply Failure (FPF) strain calculated with DDM and the FPF strain calculated using an online laminate analysis software [29] with and without in situ correction of the UD strength values.

The DDM prediction of FPF values are found to be in good agreement with the FPF values calculated using in situ strength into the Hashin damage initiation criterion implemented in the laminate analysis software [29]. The error is between 4% and 22% among 11 laminates. However, as shown in Table 3, the FPF strain is grossly underestimated if the in situ correction is neglected, with errors between 35% and 67%.

6.3 Convergence

In this section we assess the sensitivity of the DDM model to h- and p-refinement, realized by mesh refinement and by changing the element type, respectively. Reaction force vs. applied displacement for laminate 2 are reported in Fig. 18 using three discretizations, namely 1, 100, and 10,000 elements of type S4R in Abaqus. Note that the specimen is subjected to a uniform state of membrane strain, so h-refinement should not be necessary to converge on a stress field, unless the constitutive model is mesh dependent (see [20, Fig. 14]). No characteristic length has been used. The results clearly indicate the constitutive model is immune to element size.

Modulus vs. strain are reported in Figs. 12-17. It can be seen that the model predictions are not affected by the element type, namely linear S4R or quadratic S8R (compare with [20, Fig. 15]). These plots are made using just one element, taking into account that the results are insensitive to mesh refinement as discussed earlier. The material parameter G_{IC} was adjusted using Abaqus linear S4R elements. When the element is changed to Abaqus quadratic S8R, or when the DDM constitutive model is used in ANSYS with linear PLANE182 or quadratic PLANE183 elements, the predictions are not affected at all.

7 Conclusions

A novel methodology is proposed to determine the material parameters, namely the critical ERR, using laminate experimental data. It is observed that DDM predictions are good for mode I matrix cracking of Carbon-Epoxy laminates. Compared to DDM, the ply discount method overestimates the stiffness changes as a function of strain and also overestimates the asymptotic values of modulus reduction, leading to under prediction of energy dissipation (toughness). When using a strength criterion, as in the ply discount method, the need to correct the *lamina* intralaminar strength values by in situ effect is demonstrated. Also, the loss of stiffness is not complete, with stress softening not reaching zero stress even for very large strains.

The present study used crack density to identify the material parameters because the reduction of laminate modulus due to transverse matrix damage in carbon fiber laminates is small, and thus parameter identification is difficult using modulus vs. strain data. Experimental measurement of crack density vs. strain is much more sensitive to applied stress/strain than modulus. Therefore, the modeling technique must be able to predict crack density, so that it can be compared to the experimental data.

Acknowledgements

The first author wishes to express his gratitude to *Universidad Carlos III de Madrid and Banco de Santander* for their support through the “Catedra de Excelencia” award.

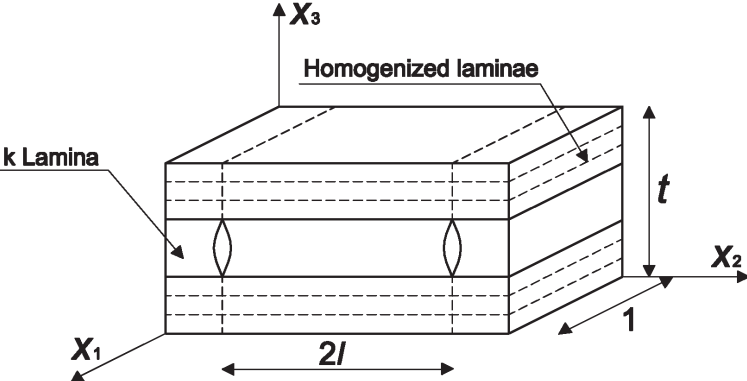


Figure 1: Representative volume element between two adjacent cracks.

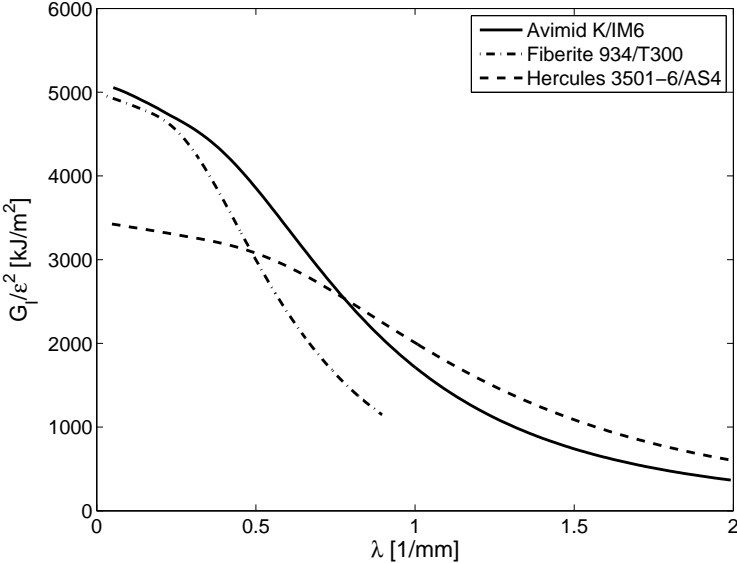


Figure 2: Calculated G_I/ϵ_x^2 vs. crack density λ .

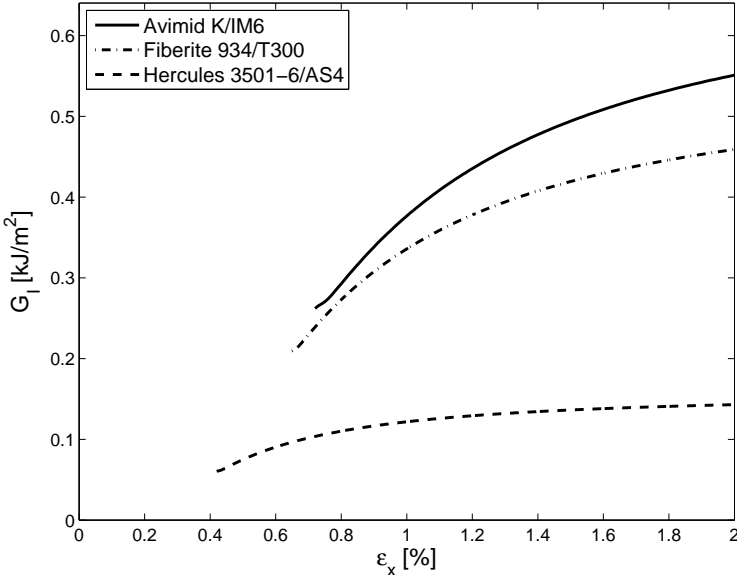


Figure 3: Calculated G_I vs. strain ϵ_x .

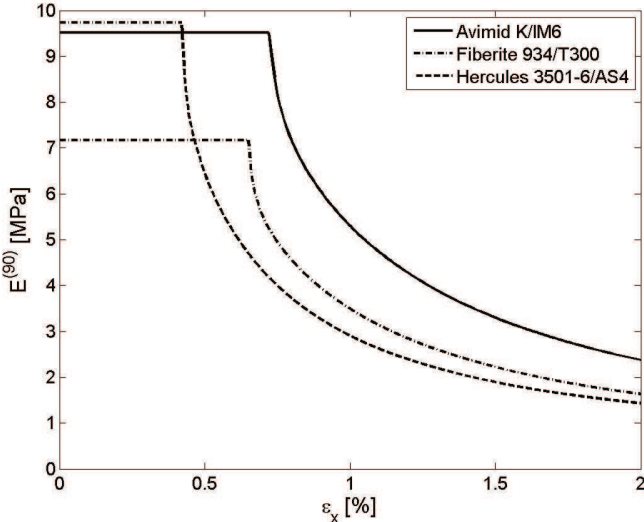


Figure 4: Modulus degradation of the cracking lamina.

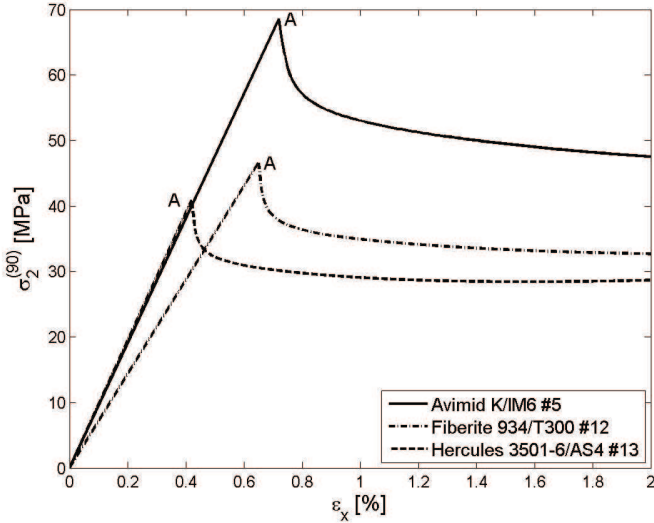


Figure 5: Stress carried by the cracking lamina.

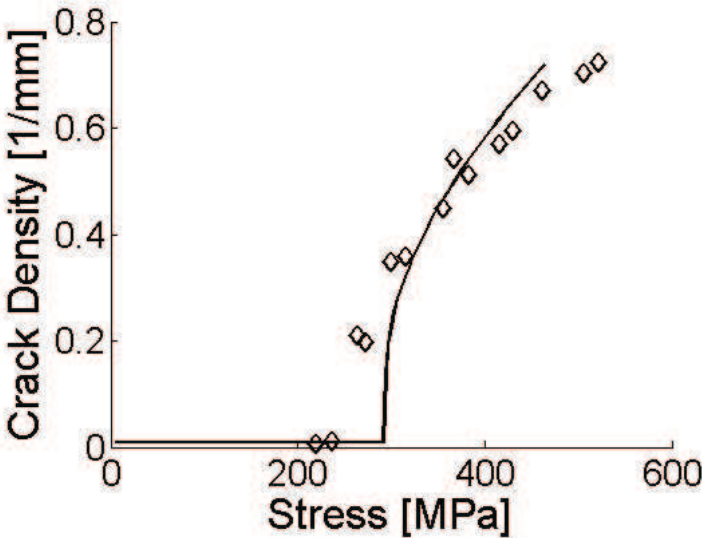


Figure 6: Avimid K/IM6 [0/90₃]_S.

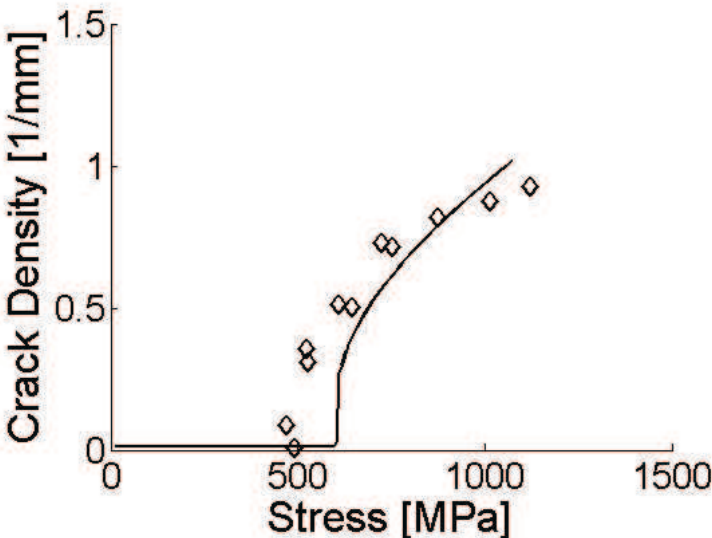


Figure 7: Avimid K/IM6 [0₂/90₂]_S.

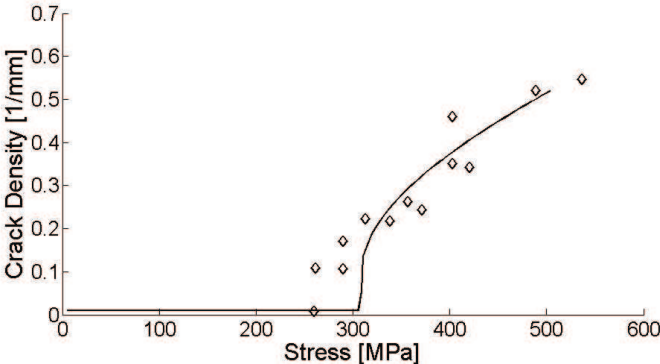


Figure 8: Fiberite 934/T300 [0₂/90₄]_S.

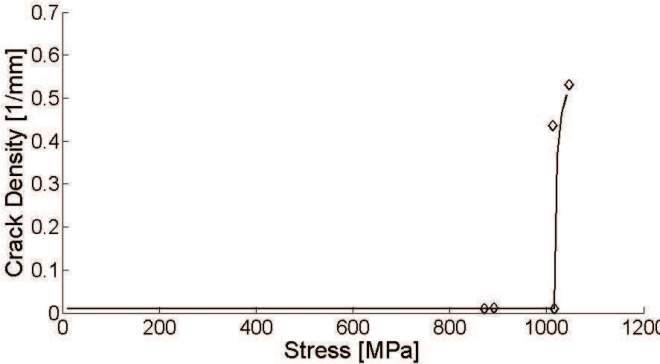


Figure 9: Fiberite 934/T300 [0₂/90]_S.

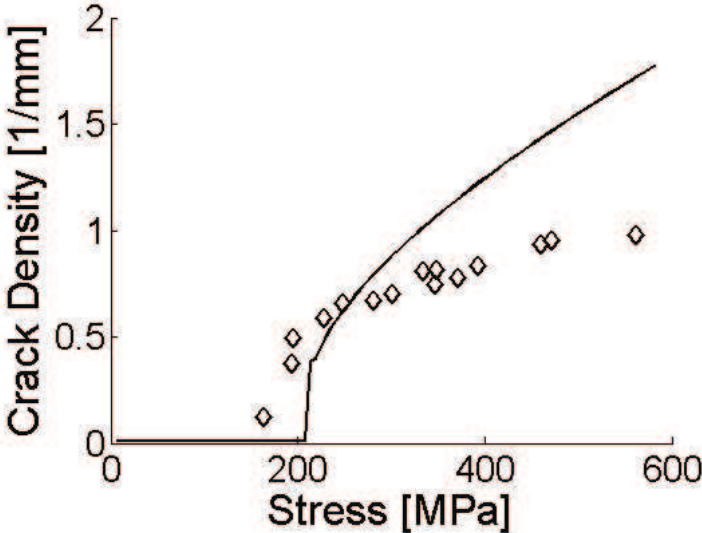


Figure 10: Hercules 3501-6/AS4 [0/90₂]_S.

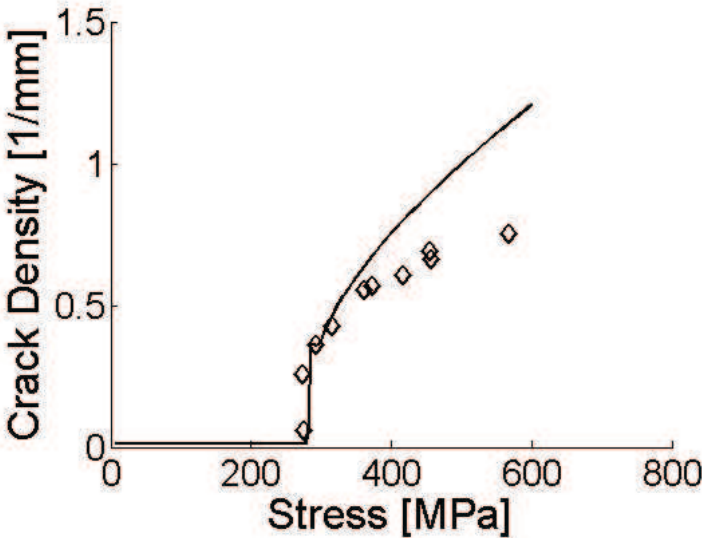


Figure 11: Hercules/AS4 [0₂/90₂]_S.

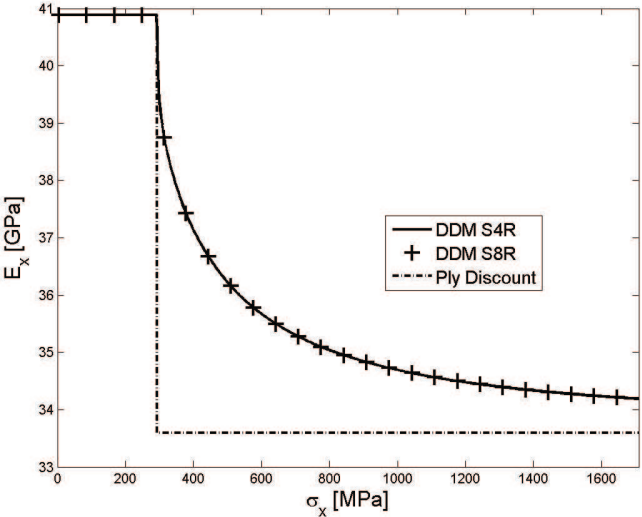


Figure 12: Avimid K/IM6 [0/90₃]_S.

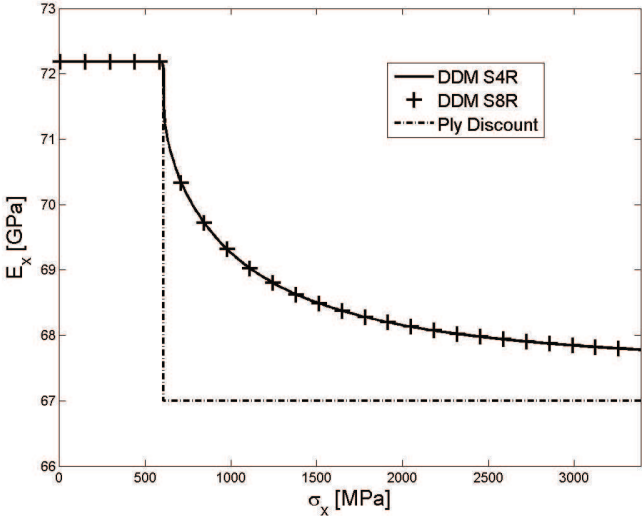


Figure 13: Avimid K/IM6 $[0_2/90_2]_S$.

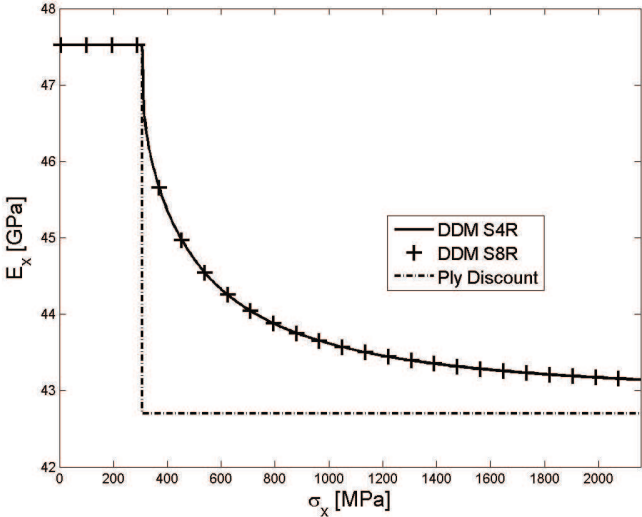


Figure 14: Fiberite 934/T300 $[0_2/90_4]_S$.

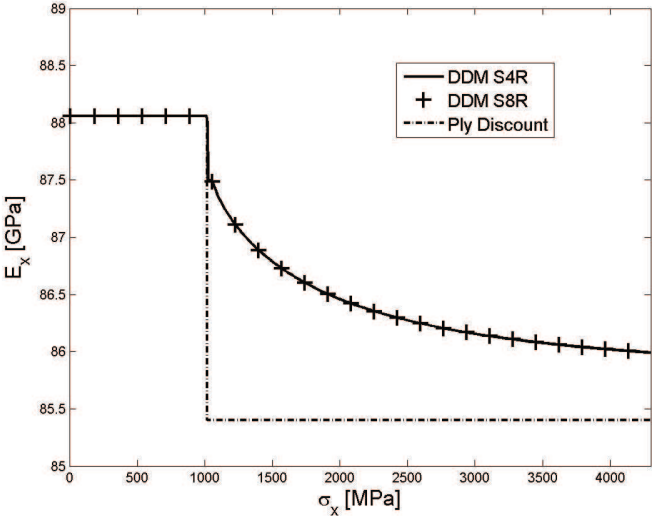


Figure 15: Fiberite 934/T300 $[0_2/90]_S$.

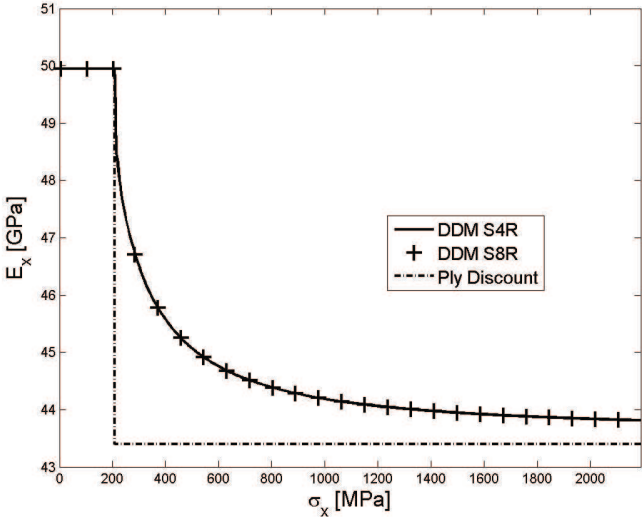


Figure 16: Hercules 3501-6/AS4 $[0/90_2]_S$.

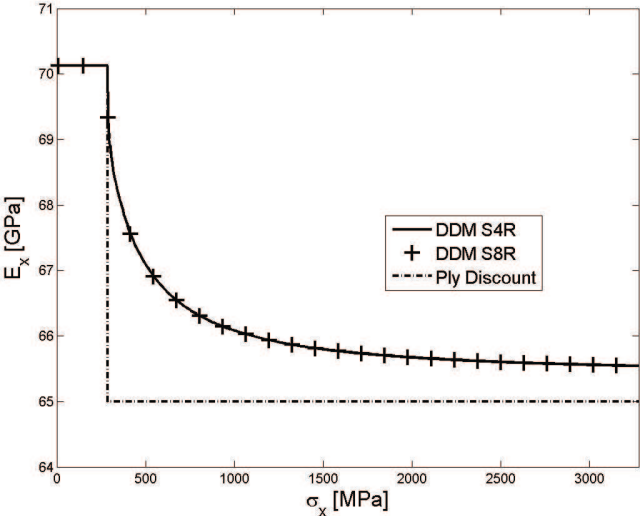


Figure 17: Hercules/AS4 $[0_2/90_2]_S$.

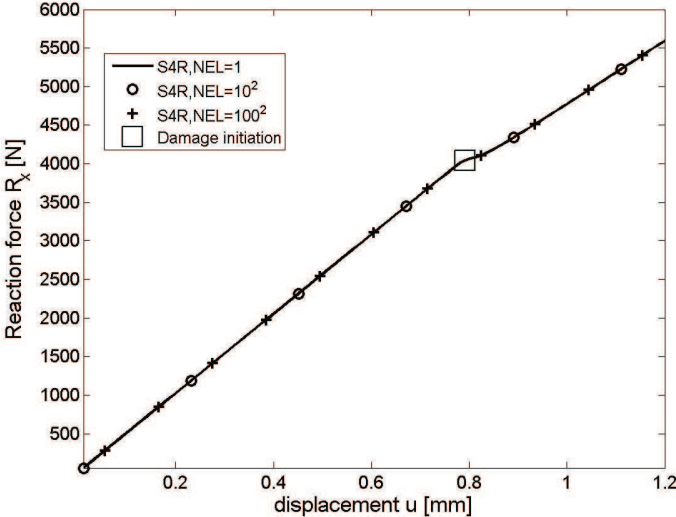


Figure 18: Force vs. displacement for laminate 2. NEL is the number of S4R elements.

Tables

Table 1: Laminates considered in this study.

Laminate	Stacking Sequence	Material
1	[0/90 ₂]s	Avimid K Polymer/IM6
2	[0/90 ₃]s	
3	[0 ₂ /90 ₂]s	
4	[0 ₂ /90 ₄]s	
5	[0/90 ₂]s	Fiberite 934/T300
6	[0/90 ₄]s	
7	[0 ₂ /90]s	
8	[0 ₂ /90 ₂]s	
9	[0 ₂ /90 ₄]s	
10	[0/90 ₂]s	Hercules 3501-6/AS4
11	[0 ₂ /90 ₂]s	

Table 2: Unidirectional ply properties [28, 32, 33].

Property	Avimid K/IM6	Fiberite 934/T300	Hercules 3501-6/AS4
E_1 [GPa]	134.0	128.0	130.0
E_2 [GPa]	9.8	7.2	9.7
G_{12} [GPa]	5.5	4.0	5.0
G_{23} [GPa]	3.6	2.4	3.6
ν_{12} [GPa]	0.3	0.3	0.3
α_1 [$\mu\epsilon/K$]	-0.09	-0.09	-0.09
α_2 [$\mu\epsilon/K$]	28.8	28.8	28.8
ply thickness [mm]	0.144	0.144	0.144
F_{1t} [MPa]	2326	1500	1950
F_{2t} [MPa]	37	27	48
F_{1c} [MPa]	1000	900	1480
F_{2c} [MPa]	200	200	200
F_6 [MPa]	63	100	79
identified (present study)			
F_{2t} [MPa]	39.8	27.6	20.2
G_{IC} [J/m ²]	258.0	208.0	60.0

Table 3: Comparison of CLT with and without in situ correction to DDM predicted FPF strain.

Laminate	E_x^0 [GPa]	E_x^∞ [GPa]	DDM [$\mu\epsilon$]	CLT [$\mu\epsilon$]			
				no in situ	% diff.	in situ	% diff.
1	51.4	44.7	8644	4078	-53	7611	-12
2	41.0	33.6	7119	4074	-43	6451	-9
3	72.2	67.0	8475	4088	-52	7631	-10
4	51.4	44.7	6271	4077	-35	6457	3
5	47.6	42.7	9153	3847	-58	7180	-22
6	31.5	25.6	6525	3834	-41	6074	-7
7	88.0	85.4	11593	3871	-67	10217	-12
8	67.9	64.0	8814	3849	-56	7186	-18
9	47.6	42.7	6525	3847	-41	6093	-7
10	50.0	43.4	4237	2090	-51	3903	-8
11	70.2	65.0	4068	2095	-49	3910	-4

References

- [1] E. J. Barbero. *Introduction to Composite Materials Design—Second Edition*. CRC Press, Philadelphia, PA, 1st edition, 2010.
- [2] R. J. Nuismer and S. C. Tan. Constitutive relations of a cracked composite lamina. *Journal of Composite Materials*, 22:306–321, 1988.
- [3] S. C. Tan and R. J. Nuismer. A theory for progressive matrix cracking in composite laminates. *Journal of Composite Materials*, 23:1029–1047, 1989.
- [4] S. Li, S. R. Reid, and P. D. Soden. A continuum damage model for transverse matrix cracking in laminated fibre-reinforced composites. *Philosophical Transactions of the Royal Society London, Series A (Mathematical, Physical and Engineering Sciences)*, 356:2379–2412, 1998.
- [5] E. Adolfsson and P. Gudmundson. Matrix crack initiation and progression in composite laminates subjected to bending and extension. *International Journal of Solids and Structures*, 36:3131–3169, 1999.
- [6] J. A. Nairn. *Polymer Matrix Composites*, volume 2 of *Comprehensive Composite Materials*, chapter Matrix Microcracking in Composites, pages 403–432. Elsevier Science, 2000.
- [7] J. M Berthelot. Transverse cracking and delamination in cross-ply glass-fiber and carbon-fiber reinforced plastic laminates: static and fatigue loading. *Applied Mechanics Review*, 56:111–147, 2003.
- [8] J. A. Nairn. *Finite Fracture Mechanics of Matrix Microcracking in Composites*, pages 207–212. Application of Fracture Mechanics to Polymers, Adhesives and Composites. Elsevier, 2004.
- [9] S. H. Lim and S. Li. Energy release rates for transverse cracking and delaminations induced by transverse cracks in laminated composites. *Composites Part A*, 36(11):1467–1476, 2005.
- [10] D. T. G. Katerelos, J. Varna, and C. Galiotis. Energy criterion for modeling damage evolution in cross-ply composite laminates. *Composites Science and Technology*, 68:2318–24, 2008.
- [11] D. T. G. Katerelos, M. Kashtalyan, C. Soutis, and C. Galiotis. Matrix cracking in polymeric composites laminates: Modeling and experiments. *Composites Science and Technology*, 68:2310–17, 2008.
- [12] Mohammed Mahdi Salavatian. Matrix damage evolution in fiber reinforced composite materials. In *SAMPE University Research Symposium*, 2013.
- [13] A. Matzenmiller, J. Lubliner, and R. Taylor. A constitutive model for anisotropic damage in fiber-composites. *Mechanics of Materials*, 20:125–152, 1995.
- [14] P. Camanho and C. Davila. Mixed-mode decohesion finite elements for the simulation of delamination in composite materials. *NASA/TM-2002-211737*, pages 1–37, 2002.
- [15] Simulia. Abaqus analysis user’s manual, version 6.12, section 24.3.
- [16] GENOA Virtual Testing & Analysis Software, Alpha STAR Corporation, <http://www.ascgenoa.com>.

- [17] Helius:MCT Composite Materials Analysis Software, Firehole Composites, <http://www.firehole.com/products/mct/>.
- [18] E. Barbero and D. Cortes. A mechanistic model for transverse damage initiation, evolution, and stiffness reduction in laminated composites. *Composites Part B*, 41:124–132, 2010.
- [19] E. J. Barbero and L. De Vivo. Constitutive model for elastic damage in fiber-reinforced pmc laminae. *International Journal of Damage Mechanics*, 10(1):73–93, 2001.
- [20] E. J. Barbero, F. A. Cosso, R. Roman, and T. L. Weadon. Determination of material parameters for Abaqus progressive damage analysis of E-Glass Epoxy laminates, <http://dx.doi.org/10.1016/j.compositesb.2012.09.069>. *Composites Part B:Engineering*, 46(3):211–220, 2012.
- [21] ANSYS Inc. Ansys mechanical apdl programmer’s manual, release 14.0, 2011.
- [22] E. J. Barbero. Finite Element Analysis of Composite Materials using Abaqus. Web resource: <http://barbero.cadec-online.com/feacm-abaqus>.
- [23] E. J. Barbero. Finite Element Analysis of Composite Materials using ANSYS. Web resource: <http://barbero.cadec-online.com/feacm-ansys>.
- [24] P. Davies. *Protocols for Interlaminar Fracture Testing of Composites*. Polymer and Composites Task Group. European Structural Integrity Society (ESIS), Plouzané, France, 1992.
- [25] R. Rikards, F.G. Buchholz, H. Wang, A.K. Bledzki, A. Korjakin, and H.A. Richard. Investigation of mixed mode i/ii interlaminar fracture toughness of laminated composites by using a cts type specimen. *Engineering Fracture Mechanics*, 61:325–342, 1998.
- [26] T. Yokozeki, T. Aoki, and T. Ishikawa. Transverse crack propagation in the specimen width direction of cfrp laminates under static tensile loadings. *Journal of Composite Materials*, 36(17):2085–99, 2002.
- [27] Z. Hashin and A. Rotem. A fatigue failure criterion for fiber-reinforced materials. *Journal of Composite Materials*, 7:448–464, 1973.
- [28] S. Liu and J. A. Nairn. Formation and propagation of matrix microcracks in cross-ply laminates. *J. Reinf. Plas. Compos.*, pages 158–178, 1992.
- [29] Computer Aided Design Environment for Composites (CADEC) <http://www.cadec-online.com>.
- [30] A. S. D. Wang. Fracture mechanics of sublaminar cracks in composite materials. *Compos. Tech. Review*, 6:45–62, 1984.
- [31] J. Lagarias, J. Reeds, M. Wright, and P. Wright. Convergence properties of the nelder-meade simplex method in low dimensions. *SIAM Journal of Optimization*, 9:112–147, 1998.
- [32] E. J. Barbero, G. Sgambitterra, A. Adumitroaie, and X. Martinez. A discrete constitutive model for transverse and shear damage of symmetric laminates with arbitrary stacking sequence. *Composite Structures*, 93:1021–1030, 2011.
- [33] E. J. Barbero. *Finite Element Analysis of Composite Materials*. Taylor & Francis, 2007.